Characterizing water solubility of fresh and aged secondary organic aerosol in PM$_{2.5}$ with the stable carbon isotope technique

Fenghua Wei[1], Xing Peng[1], Liming Cao[1], Mengxue Tang[1], Ning Feng[1], Xiaofeng Huang[1], Lingyan He[1]

[1]Laboratory of Atmospheric Observation Supersite, School of Environment and Energy, Peking University Shenzhen Graduate School, Shenzhen 518055, China.

Correspondence: Xing Peng (pengxing@pku.edu.cn)

Abstract: The investigation of the water-soluble characteristics of secondary organic carbon (SOC) is essential for a more comprehensive understanding of its climate effects. However, due to the limitations of the existing source apportionment methods, the water solubility of different types of SOC remains uncertain. This study analyzed stable carbon isotope and mass spectra signatures of total carbon (TC) and water-soluble organic carbon (WSOC) in ambient $PM_{2.5}$ samples for one year and established stable carbon isotope profiles of fresh and aged SOC. Furthermore, the Bayesian stable isotope mixing (BSIM) model was employed to reveal the water solubility characteristics of fresh and aged SOC in a coastal megacity of China. WSOC was dominated by secondary sources, with fresh and aged SOC contributing 28.1 % and 45.2 %, respectively. Water-insoluble organic carbon (WIOC) was dominated by primary sources, to which fresh and aged SOC contributed 23.2 % and 13.4 %. We also found the aging degree of SOC has considerable impacts on its water solubility due to the much higher water-soluble fraction of aged SOC (76.5 %) than fresh SOC (54.2 %). Findings of this study may provide a new perspective for further investigation of the hygroscopicity effects of SOC with different aging degrees on light extinction and climate change.

Keywords: Fresh SOC; Aged SOC; Water solubility; Stable carbon isotope; BSIM model; Mass spectrometry.

Graphical abstract:
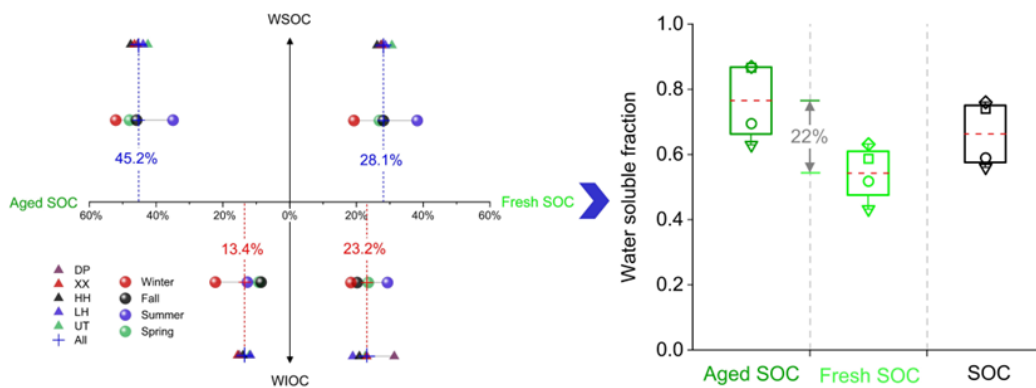
1. Introduction

As a major component of particulate matter ($PM_{2.5}$), secondary organic aerosols (SOA) not only contribute to haze formation but also exert a substantial influence on climate dynamics across various spatial scales, from local to global (Kaul et al., 2011; Shrivastava et al., 2017). The water solubility, considered one of the crucial physical properties of SOA, has been extensively studied recently due to its significant effects on the physicochemical processes in the atmosphere. The water solubility of SOA varied with its aging degrees (Kirillova et al., 2013), while both the water solubility and aging degree of organic aerosols contribute to the hygroscopicity noticeably, which affects the light extinction eventually (Han et al., 2022; Liu et al., 2022). Hence, exploring the water solubility characteristics of SOA with different aging degrees can help elucidate the more detailed extinction mechanism of SOA. In addition, recent studies have also shown that the formation of secondary particulates is one of the main processes determining the amount of cloud condensation nuclei (CCN) in remote oceanic regions (Liu and Matsui 2022). Therefore, investigating the water solubility of SOA with different aging degrees is also meaningful for further exploring its indirect climate effects.

Investigating the contributions of SOA with different aging degrees to both organic matter (OM) and water-soluble organic matter (WSOM) is imperative for determining their quantified water solubility. However, due to the constraints of reliable methods, only a limited number of studies have examined the water solubility of SOA using mass spectrometry techniques. Qiu et al. (2019) conducted source apportionment of OM in PM_1 and WSOM in $PM_{2.5}$ based on online and offline AMS-PMF methods respectively (Qiu et al., 2019). This approach faces challenges not only related to the inherent errors of online versus offline methods but also discrepancies in the measured particle sizes of OM and WSOM. Kondo et al. (2007) and Timonen et al. (2013) attempted to apportion water-soluble organic

3

49 carbon (WSOC) through a multiple linear regression method based on the mass spectral information of

50 OM, which still exhibits large indeterminateness (Timonen et al., 2013; Xiao et al., 2011; Kondo et al.,

51 2007). The carbon isotopic technique offers a promising avenue to overcome the aforementioned

52 limitations, thereby enabling a more in-depth exploration of the water-soluble characteristics of SOA.

53 Carbon isotope techniques have garnered widespread attention and are increasingly employed in source

54 apportionment studies of organic aerosols due to their robust source appointment capabilities.

55 Radioactive carbon isotopes (^{14}C) provide a precise method for quantitatively distinguishing between

56 fossil and non-fossil organic aerosol sources (Fushimi et al., 2011; Zhang et al., 2014). The stable

57 carbon isotope technique (^{13}C), however, can quantitatively assess the contributions of various sources

58 by integrating them into mass balance models (Yao et al., 2022; Widory et al., 2004). The Bayesian

59 mixing model stands out as one of the most widely utilized models (Xiao;Xu and Xiao 2023; Tang et

60 al., 2020). The stable carbon isotope technique can also be combined with other source tracers to

61 further enhance the accuracy of source apportionment of carbonaceous aerosols (Jiang et al., 2022;

62 Plasencia Sánchez et al., 2023; Ceburnis et al., 2011; Lim et al., 2022). However, to our knowledge, no

63 study has employed the carbon isotope technique to estimate the source contribution of both fresh and

64 aged SOA before, owing to the challenging measurement of the carbon isotope profiles for these two

65 sources.

66   Previous studies have predominantly concentrated on assessing the water solubility of SOA at

67 inland urban sites, revealing a strong correlation between SOA water solubility and urban air pollution

68 emissions as well as relative humidity (Wong;Zhou and Abbatt 2015; Pye et al., 2017; Favez et al.,

69 2008; Salma et al., 2007; Weber et al., 2007; Miyazaki et al., 2006). Nevertheless, few researchers have

70 noticed the differences between inland and coastal cities. As dynamic interfaces between urban and

71   marine environments (Donaldson and George 2012), coastal cities exhibit unique characteristics.

72   Shenzhen is a typical representative city for coastal air pollution studies with a coastline spanning

73   260.5 km and a total sea area of 1145 m^2. We measured the stable carbon isotope fingerprints of fresh

74   and aged secondary organic carbon (SOC), which enables us to investigate the source contributions of

75   SOC with different aging degrees to WSOC and their respective water solubility in Shenzhen.

76   The aim of this study is to investigate the water solubility of SOC in $PM_{2.5}$, emphasizing Shenzhen

77   as a representative mega-coastal city in China. We analyzed stable carbon isotopes and mass spectra

78   signatures of total carbon (TC) and WSOC in ambient $PM_{2.5}$ samples that were collected from five

79   distinct sites in Shenzhen over one year as well as specific emission sources. For the first time, we

80   employed the Bayesian stable isotope mixing (BSIM) model on localized source profiles to quantify

81   the contributions of fresh SOC and aged SOC to WSOC and water-insoluble organic carbon (WIOC).

82   These results would contribute to estimating the water solubility of both fresh and aged SOC, revealing

83   their direct or indirect implications for climate change.

84   **2. Material and methods**

85   **2.1 Ambient $PM_{2.5}$ sampling and chemical analysis**

86   Shenzhen (N22°27′ ~ N22°52′, E113°46′ ~ E114°37′), one megacity of Pearl River Delta, China, is

87   bordered by Daya Bay and Dapeng Bay to the east, the Pearl River Estuary and Lingding Sea to the

88   west, Hong Kong to the south, and Dongguan and Huizhou to the north. As a typical mega-coastal city

89   in China, Shenzhen's air quality is predominantly affected by the continental air mass from northern

90   Guangdong, the eastern coastal air mass, and the southern marine air mass (Fig. 1). For a

91   comprehensive exploration of pollution characteristics in Shenzhen, $PM_{2.5}$ samples were collected from

92 five sites covering the western to eastern regions of the city. The selected sites are Xixiang (XX, urban

93 site), University Town (UT, urban site), Longhua (LH, urban site), Honghu (HH, urban site), and

94 Dapeng (DP, background site) (Fig. 1). Additional details about each sampling site are listed in Table

95 S1.
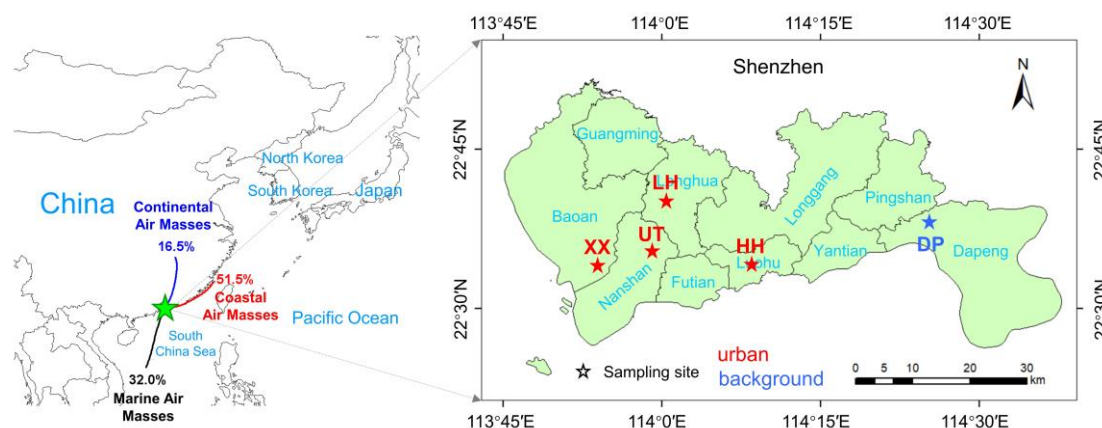
96

97 **Figure 1.** Spatial distribution of the five sampling sites in Shenzhen for this study.

98   In this study, 24-hour $PM_{2.5}$ sampling was conducted every other day in 2019 at the UT site using

99 a Thermo 2300 atmospheric particulate sampler (Thermo Fisher Scientific Inc., Waltham,

100 Massachusetts, USA), yielding a total of 160 valid samples. For the remaining four sites, a total of 295

101 valid $PM_{2.5}$ samples were collected every other day during typical months of the four seasons in 2019

102 (March, June, September, and December, Table S2) using a Model TH-16A atmospheric particulate

103 sampler (Tianhong Corp., Wuhan, China). The $PM_{2.5}$ samples collected by the quartz filter were used to

104 determine the organic carbon (OC) and elemental carbon (EC) using an OC/EC analyzer (2001A,

105 Desert Research Institute, Reno, Nevada, USA) following the IMPROVE A procedure. In addition, the

106 samples collected by Teflon filter in this study were analyzed for water-soluble ions (mainly SO_4^{2-},

107 NO_3^-, NH_4^-, and Cl^-) within $PM_{2.5}$, and the mass concentrations of twenty-three metallic elements

108 (primarily Na, Mg, Al, K, Ca, V, Fe, Ni, Zn, Pb, and Cd) within $PM_{2.5}$ were also determined using an

6

109   inductively coupled plasma mass spectrometer (ICP-MS, Aurora M90; Bruker, Germany). Relevant

110   quality control information is described in the Supplementary Information (Text S1).

111   For WSOC extraction, the $PM_{2.5}$ sample underwent ultrasonication (20 min $\times$ 3 times) in 15 ml

112   ultrapure water (18.2 MΩ·cm), followed by filtration through a syringe with a 0.45 μm filter head to

113   eliminate insoluble particles. The extracted $PM_{2.5}$ samples were sequentially analyzed using a long-

114   time-of-flight aerosol mass spectrometer (L-TOF-AMS, Aerodyne, USA) and an ultrasonic nebulizer

115   (U5000AT+, Cetac Technologies Inc., USA) to measure elemental ratios, such as O/C, as well as the

116   mass spectrum signatures of the water-soluble organic fractions, including ion fragments like CO_2^+,

117    $C_4H_9^+$, and $C_2H_4O_2^+$. The concentration of WSOC was determined using a total organic carbon analyzer

118   (multi N/C 3100, Jena, Germany), and WIOC was calculated as the difference between OC and WSOC.

119   To investigate the stable carbon isotope signatures of carbonaceous aerosols, we built a stable

120   isotope spectrometry system by integrating an OC/EC analyzer with a carbon dioxide isotope

121   spectrometer (QCLAS, Aerodyne). This system reduces the carbon requirement for isotope analysis

122   from 5 μgC to 0.5 μgC and improves the accuracy of spectroscopic measurement methods to

123   0.2‰~0.3‰. The stable carbon isotope values of TC and WSOC in ambient $PM_{2.5}$ were measured in

124   this study.

125   **2.2 Bayesian stable isotope mixing model**

126   The BSIM model could quantify the contributions of multiple sources to the TC and WSOC based on

127   the principle of mass conservation of stable isotopes, in which the Markov Chain Monte Carlo (MCMC)

128   method was employed. The methodology employed in the BSIM model was detailed in works by

129   Parnell et al. (2013) and Parnell and Inger (2010) (Parnell et al., 2010; Parnell et al., 2013). In brief, the

7

130   posterior distribution for the Bayesian neural network (BNN) was calculated utilizing the prior

131   distribution and likelihood function based on Bayes theorem. Implementation of the BSIM model in

132   this study utilized the SIMMR package in R software (https://cran.r-project.org/

133   web/packages/simmr/index.html).   Gelman diagnostic values, ranging from 1 to 1.01, all met the

134   criteria of the posterior prediction test, indicating robust model performance and reliable results.

135   Additionally, an uncertainty index (UI_{90}) was employed here to further characterize the uncertainty

136   strength of TC and WSOC source apportionments based on their posterior distribution. This index

137   refers to the difference between the proportional contributions of the maximum and minimum values in

138   the rapid increase segment divided by 90 with a 90 % cumulative probability ($UI_{90} = (PC_{95}-PC_5)/90$)

139   (Zaryab et al., 2022; Ji et al., 2017).

140   **2.3 Stable carbon isotope spectrum of $PM_{2.5}$ sources**

141   The BSIM model requires the input of potential sources for carbonaceous aerosols, along with their

142   local source-specific stable carbon isotope values (fingerprints). In this study, we firstly employed the

143   PMF model to identify the potential sources of TC and WSOC (Text S1), with the aim of reducing the

144   uncertainty of the subsequent BSIM model and verifying the reliability of the BSIM results. The PMF

145   results showed that traffic emissions, SOA, and biomass burning are the major contributors to

146   carbonaceous aerosols in Shenzhen, which were similar to the previous results in Guangzhou (Huang et

147   al., 2014). In addition, a literature review indicated that secondary conversion sources could be further

148   subdivided into fresh SOC for the low oxidation state and aged SOC for the high oxidation state (Chen

149   et al., 2019; Presto et al., 2009; Mahrt et al., 2022; Shen et al., 2017). Ultimately, traffic emissions,

150   fresh SOC, aged SOC, and biomass burning (BB) were identified as the four potential sources of TC

151   and WSOC for BSIM model in this study. Since the PMF model lacks the mass spectral information of

152   offline PM$_{2.5}$ samples, it fails to distinguish between fresh SOC and aged SOC in TC, making it

153   challenging to investigate the water solubility characteristics of the SOC based on PMF results. BSIM

154   model simultaneously quantified of fresh and aged SOC separately in both TC and WSOC, thereby

155   enabling an estimation of SOC water solubility. This capability is used for the final analysis in this

156   study.

157   Recognizing the regional variability in stable carbon isotope fingerprints of PM$_{2.5}$ sources (Yao et

158   al., 2022), this work obtained representative and locally specific carbon isotope profiles for the four

159   sources in Shenzhen. The measured profiles of the four sources were used as prior information in the

160   BSIM model for the follow-up analyses. For the traffic emissions, we measured the stable carbon

161   isotope values of TC and WSOC in PM$_{2.5}$ that were collected from the Mount Tanglang tunnel

162   (dominated by diesel vehicles) and the Jiuweiling tunnel (dominated by petrol vehicles) in Shenzhen.

163   Fresh SOC was simulated through petrol vehicle bench tests. The lowest stable carbon isotope values

164   for TC and WSOC from the simulated samples were chosen as the fresh SOC results. The oxygen-

165   carbon ratios (O/C) of fresh SOC samples in this study ranged from 0.51 to 0.62, indicating a low

166   oxidation state (Ding et al., 2012). Aged SOC samples were obtained by collecting ambient PM$_{2.5}$

167   samples at the National Ambient Air Background Monitoring Station (Mount Wuzhi site, Hainan,

168   China), primarily influenced by regional pollution transported by northern continental air masses.

169   These aged SOC samples exhibited a high O/C value of 0.98, suggesting their highly oxidized state

170   (Zhu et al., 2016). Biomass burning emissions were simulated and analyzed by burning pine wood in

171   the Laboratory of Biomass Burning Simulation at Peking University Shenzhen Graduate School (He et

172   al., 2010). Additional details about the sampling process are available in the Supplementary

173   Information (Text S2). Table 1 summarizes the stable carbon isotope fingerprints of the four sources

9

174 and f_{60} signatures used in this study. Table S3 compares $\delta^{13}C_{TC}$ source signatures in this study with

175 global datasets. The stable carbon isotope measurements from the four sources align with the range

176 observed in global datasets, thus affirming the reliability of the four source fingerprints utilized in this

177 study. Previous research identified $C_2H_4O_2^+$ (*m/z 60*) as a reliable marker for biomass burning in

178 Shenzhen, with a feature value of 1.61±0.68 % (Cao et al., 2018). This prior information was also

179 incorporated into the BSIM model to estimate the biomass burning source. Although there is some

180 overlap among the $\delta^{13}C$ fingerprints of different sources, the Bayesian approach allows for probabilistic

181 estimation of the contribution of different sources and can also integrate information from multiple

182 markers and sources to mitigate the effects of overlap. In this study, the PMF model was used to reduce

183 the uncertainty of interference from unrelated sources, and the chemical tracer marker of biomass

184 burning source (f_{60}) was also integrated to minimize the effect of this overlap.

185 **Table 1.** Stable carbon isotope fingerprints and f_{60} signatures for TC and WSOC sources.

	Traffic		Fresh SOC		Aged SOC		BB	
TC	$\delta^{13}C/‰$	$f_{60}/\%$	$\delta^{13}C/‰$	$f_{60}/\%$	$\delta^{13}C/‰$	$f_{60}/\%$	$\delta^{13}C/‰$	$f_{60}/\%$
	-26.26±0.50	0	-27.31±0.73	0	-25.54±0.28	0	-27.58±0.24	1.61±0.68
	Traffic		Fresh SOC		Aged SOC		BB	
WSOC	$\delta^{13}C/‰$	$f_{60}/\%$	$\delta^{13}C/‰$	$f_{60}/\%$	$\delta^{13}C/‰$	$f_{60}/\%$	$\delta^{13}C/‰$	$f_{60}/\%$
	-26.68±0.37	0	-26.18±0.75	0	-24.93±0.39	0	-26.78±0.17	1.61±0.68

186 **2.4 Contributions of SOC to WIOC**

187 Based on the source apportionment results from the BISM model for TC and WSOC, the contributions

188 of fresh SOC and aged SOC to WIOC were calculated according to the equations (1-2). The

189 uncertainties (u) in concentrations of Fresh SOC $_{(WIOC)}$ and Aged SOC $_{(WIOC)}$ were assessed using the

190 uncertainty transfer equations (3-4). Fresh SOC and aged SOC uncertainties in both TC (14.9 %,

191 30.1 %) and WSOC (24.1 %, 20.9 %) were determined using the BSIM model. Our findings reveal that

192   the calculated uncertainties of [Fresh SOC $_{(WIOC)}$] and [Aged SOC $_{(WIOC)}$] were 28.3 % and 36.8 %,

193   respectively.

194    $$[\text{Fresh SOC}_{(WIOC)}] = [\text{Fresh SOC}_{(TC)}] - [\text{Fresh SOC}_{(WSOC)}] \tag{1}$$

195    $$[\text{Aged SOC}_{(WIOC)}] = [\text{Aged SOC}_{(TC)}] - [\text{Aged SOC}_{(WIOC)}] \tag{2}$$

196    $$u_{[\text{Fresh SOC}_{(WIOC)}]} = \left(u^2_{[\text{Fresh SOC}_{(TC)}]} + u^2_{[\text{Fresh SOC}_{(WSOC)}]} \right)^{1/2} \tag{3}$$

197    $$u_{[\text{Aged SOC}_{(WIOC)}]} = \left(u^2_{[\text{Aged SOC}_{(TC)}]} + u^2_{[\text{Aged SOC}_{(WSOC)}]} \right)^{1/2} \tag{4}$$

198   **3. Results and discussion**

199   **3.1 Overview of PM$_{2.5}$ and carbonaceous components**

200   The annual mean concentration of PM$_{2.5}$ in Shenzhen was 24.9 μg/m^3 in 2019, with TC being the

201   predominant component, exhibiting an annual mean concentration of 7.1 μg/m^3 (5.8 and 1.3 μg/m^3 for

202   OC and EC, respectively). WSOC accounts for 48 % of OC, presenting an annual mean concentration

203   of 2.8 μg/m^3. The mean stable carbon isotope values for TC (δ^{13}C$_{TC}$) and WSOC (δ^{13}C$_{WSOC}$) were -

204   26.64 ± 0.79 ‰ and -25.80 ± 0.88 ‰, respectively, which is lower than the results of northern cities in

205   China (Wu et al., 2020). This can be attributed to the limited impact of coal combustion (which has

206   high ^{13}C values) on PM$_{2.5}$ in Shenzhen (Yao et al., 2022; Vodicka et al., 2022).

207   Seasonal variation revealed that TC, OC, WSOC, and EC exhibited elevated levels in winter and

208   decreased levels in summer (Fig. 2a). This pattern primarily stems from pollution air masses

209   originating from continental regions in the fall and winter, and clean air masses from the southern

210   ocean during the summer months (Fig. S1). The OC to EC ratio, averaging 4.5, was also higher in

211   winter than in summer, consistent with the Oxygen-to-Carbon (O/C) ratio results for WSOC (Fig. 2a),

11

212 indicating a large influence of aged SOC on carbonaceous aerosols in winter. The stable carbon isotope

213 results support this observation. Fig. 2b depicts relatively higher $\delta^{13}C_{TC}$ and $\delta^{13}C_{WSOC}$ values in spring

214 (-26.59‰, -25.26‰), fall (-26.38‰, -25.44‰), and winter (-26.46‰, -26.27‰). These higher values

215 are attributed to greater contributions of aged SOC from northern and northeast regional transport

216 processes during these seasons (Fig. S1). In summer, observed low $\delta^{13}C_{TC}$ and $\delta^{13}C_{WSOC}$ values of -

217 27.29‰ and -26.57‰, respectively, suggest relatively high contributions of fresh SOC to $PM_{2.5}$.

218 Shenzhen experiences high temperatures in summer, leading to increased gaseous precursor emissions

219 from terrestrial biogenic sources, especially C3 plants. Intense solar radiation and high temperature

220 favor photochemical reactions to generate fresh SOC that depletes ^{13}C in particulate matter during

221 summer (Kirillova et al., 2013).

222 Mass spectra characteristics of CO_2^+ (*m/z 44*), $C_4H_9^+$ (*m/z 57*), and $C_2H_4O_2^+$ (*m/z 60*) in WSOC

223 were measured to represent oxidized organic aerosol (OOA), hydrocarbon-like organic Aerosol (HOA),

224 and biomass burning organic aerosol (BBOA), respectively. The abundance of these ion fragments,

225 denoted as f_{44}, f_{57}, and f_{60}, is determined by the ratios of signal intensities at *m/z 44*, *m/z 57*, and *m/z 60*

226 to the sum of signal intensities from all *m/z* signals in the organic mass spectra. As depicted in Fig. 2c,

227 f_{44} obtained higher values in spring (0.131) and winter (0.125) compared to summer (0.120) and fall

228 (0.112), further indicating an elevated oxidation level of OOA during spring and winter. Considering

229 that f_{60} exceeds 0.0030 when biomass burning influences carbonaceous aerosol (Docherty et al., 2008;

230 DeCarlo et al., 2008), the annual average value of f_{60} was 0.0032, suggesting biomass burning was an

231 important source of carbon components in Shenzhen. Winter exhibited higher levels of f_{60} (0.0035)

232 compared to other seasons, suggesting relatively strong impacts of biomass burning on WSOC in

233 winter. Conversely, f_{57} reached its highest level in summer (0.014) and the lowest in winter (0.009),

234   with an annual average value of 0.011, possibly associated with a notable increase in hydrocarbon

235   organic aerosol emissions from traffic and biogenic sources during the summer period.
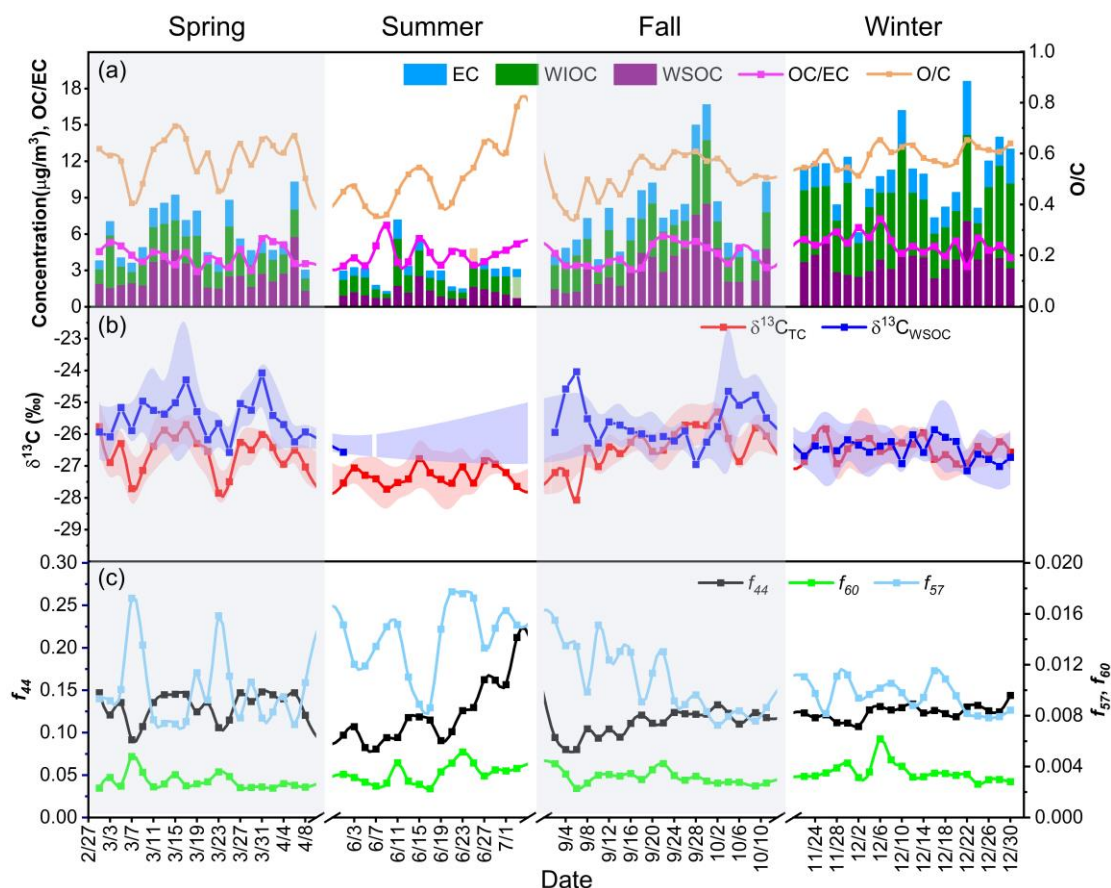

236

237   **Figure 2.** Time series of carbonaceous components (a), stable carbon isotope characteristics of TC and

238   WSOC(b), and mass spectra signatures of WSOC in $PM_{2.5}$ (c) from Shenzhen. Each data was averaged

239   from five sampling sites. (Note: Summer samples exhibit elevated analytical errors due to low

240   concentrations, and $\delta^{13}C_{WSOC}$ values are computed from combined summer samples).

241   Obvious spatial variations in $PM_{2.5}$ mass concentrations across Shenzhen during 2019 were

242   observed, with XX site registering the highest concentration (29.6 μg/m³), followed by LH (28.0

243   μg/m³), HH (23.4 μg/m³), UT (23.1 μg/m³), and DP (20.2 μg/m³). Fig. 3 illustrates that TC made more

244   substantial contributions (28.2 % ~ 32.5 %) to $PM_{2.5}$ at the four urban sites in the central and western

245   regions of Shenzhen compared to the background site (DP, 25.7 %). This suggests that local pollutant

246   emissions significantly influence carbonaceous aerosols in Shenzhen's urban areas. The percentage of

247   WSOC in TC was also higher in urban areas (37.5±3.9 %) compared to the background area (DP,

248   33.2 %), reaching the highest value at the LH site (42.9 %). However, the percentage of WIOC in TC

249   displayed the opposite trend, suggesting carbonaceous aerosols in urban areas of Shenzhen exhibit

250   higher water solubility than in background areas. Distinct spatial distribution characteristics were also

251   observed in the stable carbon isotopes of TC and WSOC. The background site exhibits higher $\delta^{13}C_{TC}$

252   values (-26.33 %) than the four urban sites (-26.72±0.13 %). This difference may be attributed to the

253   increased contribution of traffic or fresh SOC sources to carbonaceous aerosols at urban sites and the

254   relatively high contribution of aged SOC at the background site. Atmospheric aging processes of

255   organics through photochemical reactions can deplete ^{13}C in aged SOC and enrich ^{13}C in fresh SOC

256   and other related reactants simultaneously (Pavuluri and Kawamura 2017). While the close proximity

257   of the $\delta^{13}C_{WSOC}$ values at urban sites (-25.77±0.04 ‰) to the background site (DP, -25.96 ‰) suggests

258   that the WSOC in different areas of Shenzhen may share a similar origin.
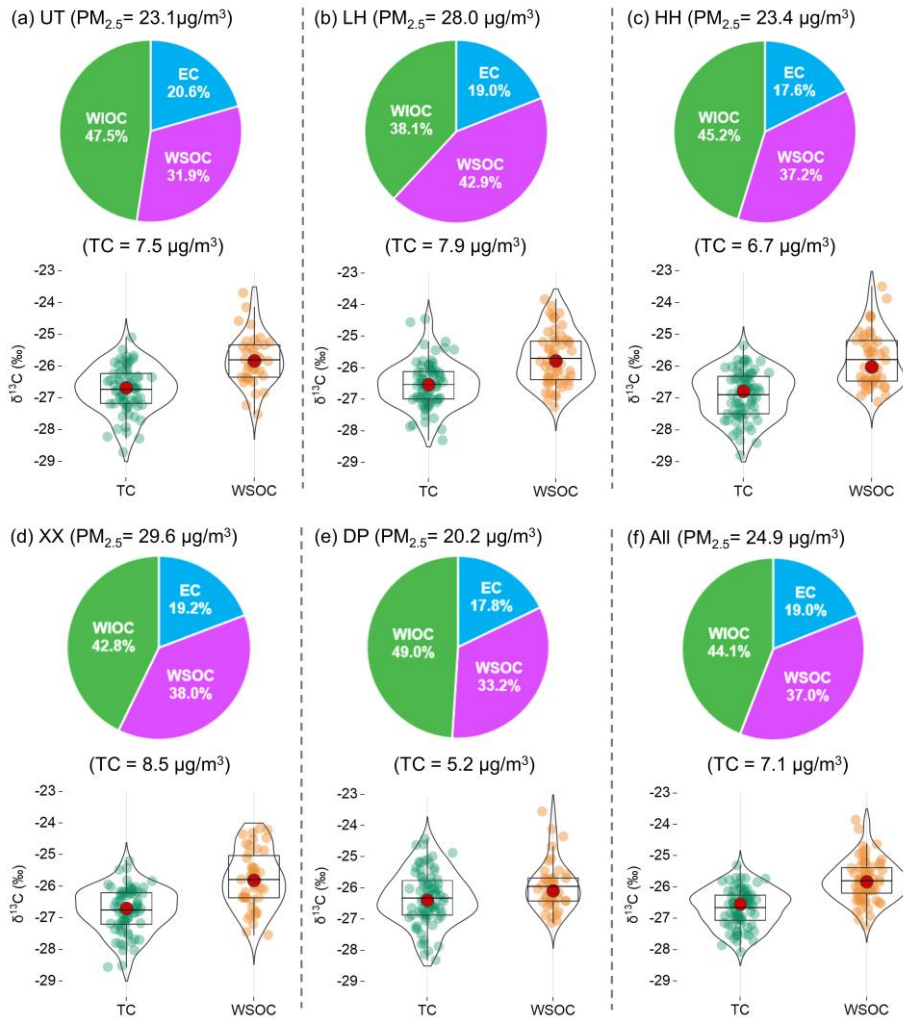
Figure 3. Chemical compositions of TC, $\delta^{13}C_{TC}$, and $\delta^{13}C_{WSOC}$ in $PM_{2.5}$ at urban sites (a-d), background site (e), and average result from all five sites (f). The Violin Box-and-Line Plots on the right display spatial variations of $\delta^{13}C_{TC}$ and $\delta^{13}C_{WSOC}$ at each site, featuring mean values (black lines) and median values (red dots).

3.2 Source apportionment results for TC and WSOC

The BSIM model assessed the contributions of traffic source, fresh SOC, aged SOC, and biomass burning (BB) to TC and WSOC, as shown in Fig. 4. On average, SOC (total of fresh and aged SOC) and traffic emerged as the two major contributors to TC, accounting for 43 % and 40 % respectively, while biomass burning contributed 17 % to TC. The contribution of aged SOC to TC (23 %) is comparable with fresh SOC (20 %). Regarding WSOC, SOC was the dominant source, comprising 45 %

270 of aged SOC and 28 % of fresh SOC, followed by BB (18 %) and Traffic (9 %). The noteworthy

271 contribution of aged SOC to WSOC suggests a comparatively higher water solubility of aged SOC in

272 Shenzhen.

273 To evaluate the BSIM model's performance, we employed the PMF model to apportion the

274 sources of TC and WSOC. The obtained results were subsequently compared with those from the

275 BSIM model, as depicted in Fig. 4a. Seventeen chemical species of $PM_{2.5}$ were applied as the PMF

276 model input to estimate source contributions to TC, encompassing carbon components, soluble

277 inorganic ions, and elements. For the apportionment of WSOC sources, five species including WSOC,

278 WIOC, and three organic mass spectra were applied as the PMF model input. More details about the

279 PMF model and results can be found in the Supplementary Information (Text S1, Fig. S2-S5). PMF

280 identified the traffic as the predominant contributor to TC (55 %), followed by SOC (34 %) and

281 biomass burning (4 %). Concerning WSOC, aged SOC and fresh SOC were the two major sources as

282 well, accounting for 43 % and 27 %, respectively. The traffic contribution to TC apportioned by the

283 PMF model is higher than that of the BSIM model (55 % vs. 40 %), which may be due to the fact that

284 some of the fresh SOC generated by the conversion of primary vehicle emissions was improperly

285 apportioned to the traffic source in the PMF model (Li et al., 2022; Zhao et al., 2014). Previous study

286 also showed that SOA contributes more to carbonaceous aerosols in Shenzhen than the traffic source

287 (Cao et al., 2022). The PMF model results for WSOC were generally consistent with BSIM model

288 results, with deviations primarily attributed to the differences in the principles and uncertainties of the

289 two models.

290 Furthermore, this study examined cumulative frequency distributions to elucidate the inherent

291   uncertainty in source apportionments of TC and WSOC. As shown in Fig. 5a and b, the proportional

292   contributions of BB source to both TC and WSOC were quite stable during the research periods due to

293   its low UI_{90} value (0.02). This may be attributed to the incorporation of mass spectral constraints for

294   the BB source in the BSIM model used in this study. For TC source apportionment results, the largest

295   UI_{90} value (0.46) was observed for the traffic source, indicating that its contribution to TC exhibited

296   relatively high uncertainty. In 90 % probability, its contribution ranged from 19.4 % to 60.9 %. The

297   UI_{90} values for fresh and aged SOC were 0.15 and 0.30, respectively. Regarding WSOC, the calculated

298   UI_{90} value of traffic, fresh SOC, and aged SOC ranged from 0.18 to 0.24. The UI_{90} values obtained

299   through the BSIM model remained within reasonable limits, and were smaller than those calculated in

300   previous related studies (0.23-0.62) (Zaryab et al., 2022; Ji et al., 2017). Consequently, the source

301   contributions of TC and WSOC estimated by the BSIM model in this study were deemed reasonable.

302   For seasonal variations, as shown in Fig. 4b, SOC still was the major source of TC and WSOC

303   during all four seasons, ranging from 38 % ~ 46 % and 71 % ~ 75 % respectively. Significant high

304   contributions of fresh SOC to TC and WSOC occurred in summer (27 %, 39 %), and relatively higher

305   contributions of aged SOC to TC and WSOC were observed in winter (26 %, 52 %). It is because

306   meteorological conditions in winter characterized by inversions and stagnant winds facilitate the

307   accumulation of air pollutants, and Shenzhen is largely influenced by regional pollution transport in

308   winter, favoring the formation of aged SOC (Huang et al., 2018). In contrast, favorable meteorological

309   conditions (e.g. intense and prolonged solar radiation, high temperatures, and relative humidity) in

310   summer enhanced photochemical reactions to generate fresh SOC. In terms of spatial distributions (Fig.

311   4c), the contributions of the traffic source to TC were higher at urban sites (38 % to 43 %) compared to

312   the background site (34 %). This finding aligns with expectations due to increased human activity and

vehicle numbers in urban locations. At the DP site, the contributions of SOC to TC were higher than those of other sources (47 %), signifying a predominant influence of regionally transported pollutant emissions on TC at the background site. However, the contributions of SOC and the other two primary sources at both urban and background sites were all close to each other, indicating the source composition of WSOC in Shenzhen is less affected by air pollution degree compared to TC.
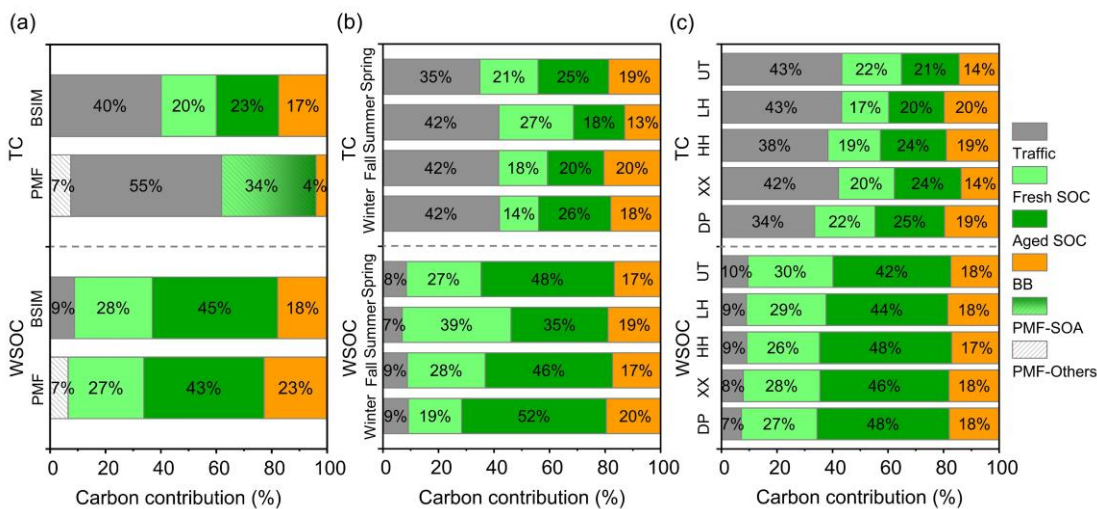
Figure 4. (a) Comparison of source apportionment results between BSIM model and PMF model for TC and WSOC, (b) seasonal and (c) spatial distributions of source apportionment results for TC and WSOC based on the BSIM model.
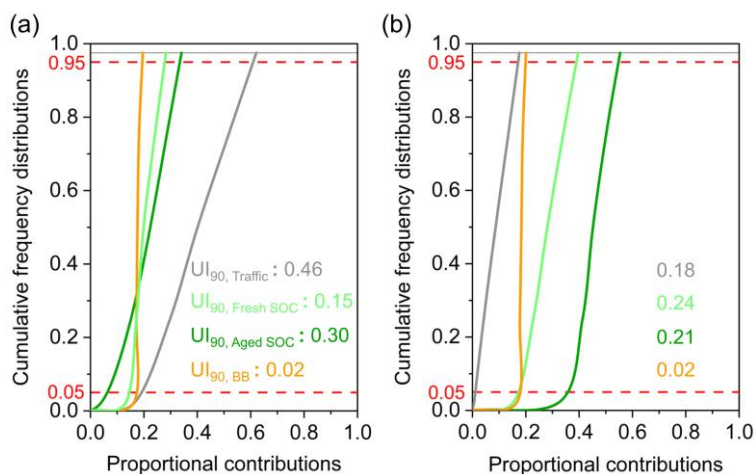
Figure 5. Cumulative frequency distributions of the proportional contributions from potential sources of TC (a) and WSOC (b) based on BSIM model.

3.3 Water solubility of fresh SOC and aged SOC

The contributions of fresh SOC and aged SOC to WIOC were the differences between the contributions

of those two SOC sources to TC and WSOC from the BSIM model (Sect. 2.4) in this study. As shown

in Fig. 6a, fresh SOC and aged SOC made contributions of 23.2±4.2 % and 13.4±3.8 % to WIOC,

respectively, implying that primary sources are the dominant contributors to WIOC. Further support for

this finding is evident in the strong correlation between WIOC and EC, as depicted in Fig. 6b. A higher

slope was observed in winter (2.4) than in other seasons, consistent with the highest contributions of

aged SOC to WIOC in winter (22 %). This observation implies that WIOC in winter is influenced not

only by local primary sources but also by the promotion of secondary pollution.

To investigate deeply the water solubility characteristics of fresh and aged SOC, we then calculate

their water-soluble fraction by comparing their water-soluble portion to the ambient fraction ($[c]_{water\text{-}soluble}/([c]_{water\text{-}soluble} + [c]_{water\text{-}insoluble})$, where $[c]_{water\text{-}soluble}$ and $[c]_{water\text{-}insoluble}$ are the concentrations of fresh

SOC or aged SOC in WSOC and WIOC, respectively) (Li et al., 2021). As shown in Fig. 6c, the overall

water-soluble fraction of SOC in this study was 66.2 % with a range from 58.9 % to 76.0 %. Fresh

SOC exhibited a much lower water-solubility of 54.2 %, whereas aged SOC displayed a comparatively

higher water-solubility of 76.5 %. The higher water solubility of aged SOC compared to fresh SOC

might be due to the positive correlation between aerosol hygroscopicity and oxidation in the sub-

saturated state. The water-soluble fraction of SOC in this study was close to that reported in other

coastal cities (Tokyo (71 %) and Southeastern United States (60 %)) (Kondo et al., 2007; Verma et al.,

2015), while was much higher than that reported in northern Chinese cities (Beijing (42 % ~ 45 %) and

Handan (49 %)) (Li et al., 2021; Qiu et al., 2019). In addition, the water-soluble fraction of both fresh

SOC and aged SOC, as calculated in this study, was comparable to that reported in Guangzhou (61 %

347 and 86 % for fresh and aged SOC respectively) (Xiao et al., 2011). This could be attributed to

348 Shenzhen's coastal location, which is markedly influenced by regional transport from neighboring

349 urban areas and the eastern seaboard air masses. The high relative humidity facilitates the conversion of

350 aged SOC into WSOC during the pollution transport process. This result is in accordance with previous

351 findings that air masses influenced by anthropogenic emissions could promote the formation of high

352 water-soluble SOA under high relative humidity in urban environments (Miyazaki et al., 2006; Salma

353 et al., 2007; Weber et al., 2007). Given that the aging process of SOA dissolved in water could enhance

354 the cloud condensation nuclei (CCN) activity of the particles (Liu and Matsui 2022), high water-

355 soluble aged SOC in Shenzhen might have significant impacts on the activity of CCN, potentially

356 resulting in more important indirect climate effects.

357 The water-soluble fraction of SOC (especially aged SOC) in Shenzhen exhibits obvious seasonal

358 characteristics, with the highest in fall (76.0 %) and the lowest in winter (56.0 %). This phenomenon is

359 primary related to the robust atmospheric oxidizing capacity during fall in Shenzhen since the

360 atmospheric oxidants such as OH and NO_3 radicals play pivotal roles in driving the secondary

361 generation of WSOC (Wang et al., 2023). Conversely, during winter, the temperature and relative

362 humidity are at their lowest levels, and the relatively diminished atmospheric oxidizing capacity also

363 constrains the secondary generation of WSOC.
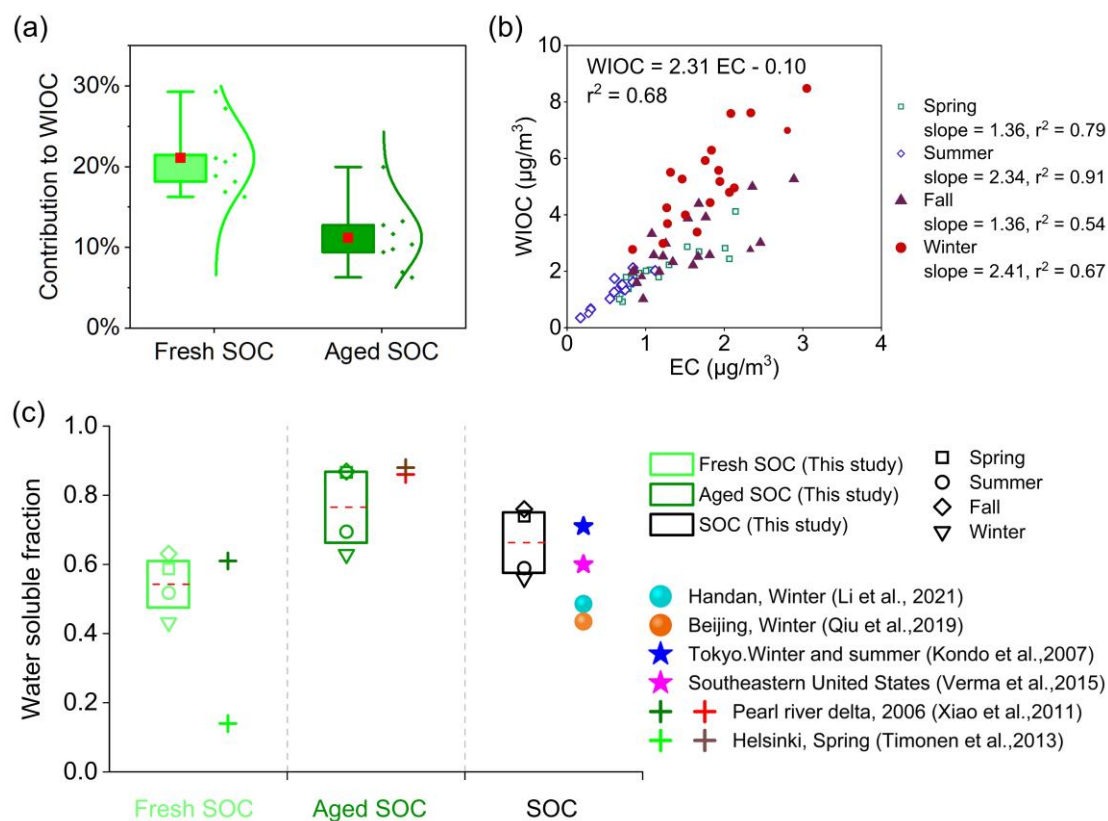
Figure 6. (a) Left is the box and whisker plots of fresh and aged SOC contributions to WIOC, the upper and lower of the box representing the 75th and 25th percentiles, and the red squares featuring mean values. The dots on the right show the contribution of fresh and aged SOC to WIOC across seasons and sites, the curve demonstrates its normal distribution. (b) Scatterplot of WIOC versus EC by season, (c) Comparison of the water-soluble fraction of SOC (fresh SOC, aged SOC, SOC) in this study (box and whisker plots) with those in other related literature (colored markings on the right). The upper and lower of the box represent the 75th and 25th percentiles and the dashed red lines indicate mean values.

4. Summary and implications

Assessing the impacts of different oxidational SOC on air quality and its water solubility has been challenging, and this work successfully evaluated the water-soluble fraction of fresh and aged SOC employing the BSIM model on one-year observational data for stable carbon isotopes and mass spectra of TC and WSOC in Shenzhen, China. Compared with other methods, e.g. PMF model, EC tracer, and

21

378 multiple linear regression analyses, the BSIM model successfully calculated the contributions of fresh

379 SOC and aged SOC to WSOC and WIOC, owing to prior and localized information about stable carbon

380 isotopes and mass spectra of $PM_{2.5}$ sources. Therefore, establishing localized carbonaceous aerosol

381 source profiles for stable carbon isotopes becomes crucial for comprehending the relationship between

382 the aging degree and water solubility of SOC.

383   The observed average mass concentration of $PM_{2.5}$ during the sampling period in Shenzhen was

384 24.9 μg/m^3, and WSOC accounts for 48 % of OC. The mean stable carbon isotope values for TC

385 ($\delta^{13}C_{TC}$) and WSOC ($\delta^{13}C_{WSOC}$) were -26.64 ± 0.79 ‰ and -25.80 ± 0.88 ‰, respectively. WSOC was

386 dominated by secondary sources while WIOC was dominated by primary sources. The contribution of

387 fresh SOC and aged SOC to WSOC, WIOC were 28.1 % and 45.2 %, 23.2 % and 13.4 %, respectively.

388 The overall water-soluble fraction of SOC in this study was 66.2 %, with aged SOC constituting 76.5 %

389 and fresh SOC 54.2 %. The water-soluble fraction of aged SOC was 22 % higher than fresh SOC, even

390 though both of them demonstrated remarkable water-soluble characteristics in Shenzhen. This finding

391 highlights the important role of aged SOC in the water uptake process of particulate matter.

392 Considering the strong correlation between the water solubility of SOC and its light extinction effect,

393 further exploration of the extinction effect of SOC with different aging degrees will greatly contribute

394 to a more profound understanding of the extinction mechanism of SOC. Besides, the water solubility of

395 SOC in coastal cities was observed to be higher than that in inland cities, suggesting a more

396 pronounced climate effect of SOC in coastal cities. Therefore, there should be increased emphasis on

397 enhancing the control of SOA precursors in coastal urban areas to better integrate air pollution and

398 climate change management. This is particularly crucial given the observed rise in the proportion of

399 SOA in particulate matter in recent years. Moreover, the results of our study further hinted that the

400   notable water solubility of SOC, particularly aged SOC, may contribute a lot to the formation of CCN

401   above coastal cities, which is also helpful to a better understanding of the cloud microphysical

402   processes and the indirect climate effect of SOC in coastal urban regions.

416 **References**

417 Cao, L. M., Huang, X. F., Li, Y. Y., Hu, M. & He, L. Y. (2018) Volatility measurement of

418   atmospheric submicron aerosols in an urban atmosphere in southern China. *Atmos. Chem.*

419   *Phys.,* 18, 1729-1743.

420 Cao, L. M., Wei, J., He, L. Y., Zeng, H., Li, M. L., Zhu, Q., Yu, G. H. & Huang, X. F. (2022)

421   Aqueous aging of secondary organic aerosol coating onto black carbon: Insights from

422   simultaneous L-ToF-AMS and SP-AMS measurements at an urban site in southern China. *J.*

423   *Clean. Prod.,* 330.

424 Ceburnis, D., Garbaras, A., Szidat, S., Rinaldi, M., Fahrni, S., Perron, N., Wacker, L., Leinert, S.,

425   Remeikis, V., Facchini, M. C., Prevot, A. S. H., Jennings, S. G., Ramonet, M. & O'Dowd, C.

426   D. (2011) Quantification of the carbonaceous matter origin in submicron marine aerosol by

427   13C and 14C isotope analysis. *Atmos. Chem. Phys.,* 11, 8593-8606.

428 Chen, T., Liu, Y., Chu, B., Liu, C., Liu, J., Ge, Y., Ma, Q., Ma, J. & He, H. (2019) Differences of

429   the oxidation process and secondary organic aerosol formation at low and high precursor

430   concentrations. *J Environ Sci (China).* 79, 256-263.

431 DeCarlo, P. F., Dunlea, E. J., Kimmel, J. R., Aiken, A. C., Sueper, D., Crounse, J., Wennberg, P. O.,

432   Emmons, L., Shinozuka, Y., Clarke, A., Zhou, J., Tomlinson, J., Collins, D. R., Knapp, D.,

433   Weinheimer, A. J., Montzka, D. D., Campos, T. & Jimenez, J. L. (2008) Fast airborne aerosol

434   size and chemistry measurements above Mexico City and Central Mexico during the

435   MILAGRO campaign. *Atmos. Chem. Phys.,* 8, 4027-4048.

436 Ding, X., Wang, X. M., Gao, B., Fu, X. X., He, Q. F., Zhao, X. Y., Yu, J. Z. & Zheng, M. (2012)

437   Tracer-based estimation of secondary organic carbon in the Pearl River Delta, south China. *J.*

438   *Geophys. Res. Atmos.,* 117, 1-14.

439   Docherty, K. S., Stone, E. A., Ulbrich, I. M., DeCarlo, P. F., Snyder, D. C., Schauer, J. J., Peltier, R.

440   E., Weber, R. J., Murphy, S. M., Seinfeld, J. H., Grover, B. D., Eatough, D. J. & Jimenez, J. L.

441   (2008) Apportionment of primary and secondary organic aerosols in Southern California

442   during the 2005 study of organic aerosols in riverside (SOAR-1). *Environ. Sci. Technol.,* 42,

443   7655-7662.

444   Donaldson, D. J. & George, C. (2012) Sea-surface chemistry and its impact on the marine

445   boundary layer. *Environ. Sci. Technol.,* 46, 10385-10389.

446   Favez, O., Sciare, J., Cachier, H., Alfaro, S. C. & Abdelwahab, M. M. (2008) Significant

447   formation of water-insoluble secondary organic aerosols in semi-arid urban environment.

448   *Geophys. Res. Lett.,* 35.

449   Fushimi, A., Wagai, R., Uchida, M., Hasegawa, S., Takahashi, K., Kondo, M., Hirabayashi, M.,

450   Morino, Y., Shibata, Y., Ohara, T., Kobayashi, S. & Tanabe, K. (2011) Radiocarbon (14C)

451   diurnal variations in fine particles at sites downwind from Tokyo, Japan in summer. *Environ.*

452   *Sci. Technol.,* 45, 6784-92.

453   Han, S., Hong, J., Luo, Q., Xu, H., Tan, H., Wang, Q., Tao, J., Zhou, Y., Peng, L., He, Y., Shi, J.,

454   Ma, N., Cheng, Y. & Su, H. (2022) Hygroscopicity of organic compounds as a function of

455   organic functionality, water solubility, molecular weight, and oxidation level. *Atmos. Chem.*

456   *Phys.,* 22, 3985-4004.

457   He, L. Y., Lin, Y., Huang, X. F., Guo, S., Xue, L., Su, Q., Hu, M., Luan, S. J. & Zhang, Y. H. (2010)

458   Characterization of high-resolution aerosol mass spectra of primary organic aerosol

459   emissions from Chinese cooking and biomass burning. *Atmos. Chem. Phys.,* 10, 11535-11543.

460   Huang, R. J., Zhang, Y., Bozzetti, C., Ho, K. F., Cao, J. J., Han, Y., Daellenbach, K. R., Slowik, J.

461   G., Platt, S. M., Canonaco, F., Zotter, P., Wolf, R., Pieber, S. M., Bruns, E. A., Crippa, M.,

462   Ciarelli, G., Piazzalunga, A., Schwikowski, M., Abbaszade, G., Schnelle-Kreis, J.,

463   Zimmermann, R., An, Z., Szidat, S., Baltensperger, U., El Haddad, I. & Prevot, A. S. (2014)

464   High secondary aerosol contribution to particulate pollution during haze events in China.

465   *Nature.,* 514, 218-22.

466   Huang, X. F., Zou, B. B., He, L. Y., Hu, M., Prévôt, A. S. H. & Zhang, Y. H. (2018) Exploration of

467   PM2.5 sources on the regional scale in the Pearl River Delta based on ME-2 modeling. *Atmos.*

468   *Chem. Phys.,* 18, 11563-11580.

469   Ji, X. L., Xie, R. T., Hao, Y. & Lu, J. (2017) Quantitative identification of nitrate pollution sources

470   and uncertainty analysis based on dual isotope approach in an agricultural watershed. *Environ.*

471   *Pollut.,* 229, 586-594.

472   Jiang, F., Liu, J., Cheng, Z., Ding, P., Xu, Y., Zong, Z., Zhu, S., Zhou, S., Yan, C., Zhang, Z.,

473   Zheng, J., Tian, C., Li, J. & Zhang, G. (2022) Dual-carbon isotope constraints on source

474   apportionment of black carbon in the megacity Guangzhou of the Pearl River Delta region,

475   China for 2018 autumn season. *Environ. Pollut.,* 294, 118638.

476   Kaul, D. S., Gupta, T., Tripathi, S. N., Tare, V. & Collett, J. L. (2011) Secondary organic aerosol: a

477   comparison between foggy and nonfoggy days. *Environ. Sci. Technol.,* 45, 7307-7313.

478   Kirillova, E. N., Andersson, A., Sheesley, R. J., Kruså, M., Praveen, P. S., Budhavant, K., Safai, P.

479   D., Rao, P. S. P. & Gustafsson, Ö. (2013) 13C- and 14C-based study of sources and

480   atmospheric processing of water-soluble organic carbon (WSOC) in South Asian aerosols. *J.*

481   *Geophys. Res. Atmos.,* 118, 614-626.

482   Kondo, Y., Miyazaki, Y., Takegawa, N., Miyakawa, T., Weber, R. J., Jimenez, J. L., Zhang, Q. &

483   Worsnop, D. R. (2007) Oxygenated and water-soluble organic aerosols in Tokyo. *J. Geophys.*

484   *Res. Atmos.,* 112.

485   Li, H., Zhang, Q., Jiang, W., Collier, S., Sun, Y., Zhang, Q. & He, K. (2021) Characteristics and

486   sources of water-soluble organic aerosol in a heavily polluted environment in Northern China.

487   *Sci. Total Environ.,* 758, 143970.

488   Li, S. Y., Liu, D. T., Kong, S. F., Wu, Y. Z., Hu, K., Zheng, H., Cheng, Y., Zheng, S. R., Jiang, X.

489   T., Ding, S., Hu, D. W., Liu, Q., Tian, P., Zhao, D. L. & Sheng, J. J. (2022) Evolution of

490   source attributed organic aerosols and gases in a megacity of central China. *Atmos. Chem.*

491   *Phys.,* 22, 6937-6951.

492   Lim, S., Hwang, J., Lee, M., Czimczik, C. I., Xu, X. & Savarino, J. (2022) Robust Evidence of

493   14C, 13C, and 15N Analyses Indicating Fossil Fuel Sources for Total Carbon and

494   Ammonium in Fine Aerosols in Seoul Megacity. *Environ. Sci. Technol.,* 56, 6894-6904.

495   Liu, L., Kuang, Y., Zhai, M., Xue, B., He, Y., Tao, J., Luo, B., Xu, W., Tao, J., Yin, C., Li, F., Xu,

496   H., Deng, T., Deng, X., Tan, H. & Shao, M. (2022) Strong light scattering of highly

497   oxygenated organic aerosols impacts significantly on visibility degradation. *Atmos. Chem.*

498   *Phys.,* 22, 7713-7726.

499   Liu, M. X. & Matsui, H. (2022) Secondary organic aerosol formation regulates cloud

500   condensation nuclei in the global remote troposphere. *Geophys. Res. Lett.,* 49.

501   Mahrt, F., Peng, L., Zaks, J., Huang, Y., Ohno, P. E., Smith, N. R., Gregson, F. K. A., Qin, Y.,

502   Faiola, C. L., Martin, S. T., Nizkorodov, S. A., Ammann, M. & Bertram, A. K. (2022) Not all

503   types of secondary organic aerosol mix: two phases observed when mixing different

504   secondary organic aerosol types. *Atmos. Chem. Phys.,* 22, 13783-13796.

505   Miyazaki, Y., Kondo, Y., Takegawa, N., Komazaki, Y., Fukuda, M., Kawamura, K., Mochida, M.,

506   Okuzawa, K. & Weber, R. J. (2006) Time-resolved measurements of water-soluble organic

507   carbon in Tokyo. *J. Geophys. Res. Atmos.,* 111.

508   Parnell, A. C., Inger, R., Bearhop, S. & Jackson, A. L. (2010) Source partitioning using stable

509   isotopes: coping with too much variation. *PLoS One.,* 5, e9672.

510   Parnell, A. C., Phillips, D. L., Bearhop, S., Semmens, B. X., Ward, E. J., Moore, J. W., Jackson, A.

511   L., Grey, J., Kelly, D. J. & Inger, R. (2013) Bayesian stable isotope mixing models.

512   *Environmetrics.,* 24, 387-399.

513   Pavuluri, C. M. & Kawamura, K. (2017) Seasonal changes in TC and WSOC and their 13C

514   isotope ratios in Northeast Asian aerosols: land surface-biosphere-atmosphere interactions.

515   *Acta Geochimica,* 36, 355-358.

516   Plasencia Sánchez, E., Sánchez-Soberón, F., Rovira, J., Sierra, J., Schuhmacher, M., Soler, A.,

517   Torrentó, C. & Rosell, M. (2023) Integrating dual C and N isotopic approach to elemental

518   and mathematical solutions for improving the PM source apportionment in complex urban

519   and industrial cities: Case of Tarragona - Spain. *Atmos. Environ.,* 293.

520   Presto, A., Miracolo, M., Kroll, J., Worsnop, D., Robinson, A. & Donahue, N. (2009)

521   Intermediate-volatility organic compounds: a potential source of ambient oxidized organic

522   aerosol. *Environ. Sci. Technol.,* 43, 4744–4749.

523   Pye, H. O. T., Murphy, B. N., Xu, L., Ng, N. L., Carlton, A. G., Guo, H., Weber, R., Vasilakos, P.,

524   Appel, K. W., Budisulistiorini, S. H., Surratt, J. D., Nenes, A., Hu, W., Jimenez, J. L.,

525   Isaacman-VanWertz, G., Misztal, P. K. & Goldstein, A. H. (2017) On the implications of

526   aerosol liquid water and phase separation for organic aerosol mass. *Atmos. Chem. Phys.,* 17,

527   343-369.

528   Qiu, Y., Xie, Q., Wang, J., Xu, W., Li, L., Wang, Q., Zhao, J., Chen, Y., Chen, Y., Wu, Y., Du, W.,

529   Zhou, W., Lee, J., Zhao, C., Ge, X., Fu, P., Wang, Z., Worsnop, D. R. & Sun, Y. (2019)

530   Vertical characterization and source apportionment of water-soluble organic aerosol with

531   high-resolution aerosol mass spectrometry in Beijing, China. *ACS Earth Space Chem.,* 3,

532   273-284.

533   Salma, I., Ocskay, R., Chi, X. & Maenhaut, W. (2007) Sampling artefacts, concentration and

534   chemical composition of fine water-soluble organic carbon and humic-like substances in a

535   continental urban atmospheric environment. *Atmos. Environ.,* 41, 4106-4118.

536   Shen, Z., Zhang, Q., Cao, J., Zhang, L., Lei, Y., Huang, Y., Huang, R. J., Gao, J., Zhao, Z., Zhu, C.,

537   Yin, X., Zheng, C., Xu, H. & Liu, S. (2017) Optical properties and possible sources of brown

538   carbon in PM2.5 over Xi'an, China. *Atmos. Environ.,* 150, 322-330.

539   Shrivastava, M., Cappa, C. D., Fan, J. W., Goldstein, A. H., Guenther, A. B., Jimenez, J. L., Kuang,

540   C., Laskin, A., Martin, S. T., Ng, N. L., Petaja, T., Pierce, J. R., Rasch, P. J., Roldin, P.,

541   Seinfeld, J. H., Shilling, J., Smith, J. N., Thornton, J. A., Volkamer, R., Wang, J., Worsnop, D.

542   R., Zaveri, R. A., Zelenyuk, A. & Zhang, Q. (2017) Recent advances in understanding

543   secondary organic aerosol: Implications for global climate forcing. *Rev. Geophys.,* 55, 509-

544   559.

545   Tang, T., Cheng, Z., Xu, B., Zhang, B., Zhu, S., Cheng, H., Li, J., Chen, Y. & Zhang, G. (2020)

546   Triple Isotopes δ13C, δ2H, and δ14C Compositions and Source Apportionment of

547   Atmospheric Naphthalene: A Key Surrogate of Intermediate-Volatility Organic Compounds

548   (IVOCs). *Environ. Sci. Technol.,* 54, 5409-5418.

549   Timonen, H., Carbone, S., Aurela, M., Saarnio, K., Saarikoski, S., Ng, N. L., Canagaratna, M. R.,

550   Kulmala, M., Kerminen, V.-M., Worsnop, D. R. & Hillamo, R. (2013) Characteristics,

551   sources and water-solubility of ambient submicron organic aerosol in springtime in Helsinki,

552   Finland. *J Aerosol Sci.,* 56, 61-77.

553   Verma, V., Fang, T., Xu, L., Peltier, R. E., Russell, A. G., Ng, N. L. & Weber, R. J. (2015) Organic

554   aerosols associated with the generation of reactive oxygen species (ROS) by water-soluble

555   PM2.5. *Environ. Sci. Technol.,* 49, 4646-56.

556   Vodicka, P., Kawamura, K., Schwarz, J. & Zdimal, V. (2022) Seasonal changes in stable carbon

557   isotopic composition in the bulk aerosol and gas phases at a suburban site in Prague. *Sci.*

558   *Total Environ.,* 803, 149767.

559   Wang, Y., Feng, Z., Yuan, Q., Shang, D., Fang, Y., Guo, S., Wu, Z., Zhang, C., Gao, Y., Yao, X.,

560   Gao, H. & Hu, M. (2023) Environmental factors driving the formation of water-soluble

561   organic aerosols: A comparative study under contrasting atmospheric conditions. *Sci. Total*

562   *Environ.,* 866, 161364.

563   Weber, R. J., Sullivan, A. P., Peltier, R. E., Russell, A., Yan, B., Zheng, M., de Gouw, J., Warneke,

564   C., Brock, C., Holloway, J. S., Atlas, E. L. & Edgerton, E. (2007) A study of secondary

565   organic aerosol formation in the anthropogenic-influenced southeastern United States. *J.*

566   *Geophys. Res. Atmos.,* 112.

567   Widory, D., Roy, S., Le Moullec, Y., Goupil, G., Cocherie, A. & Guerrot, C. (2004) The origin of

568   atmospheric particles in Paris: a view through carbon and lead isotopes. *Atmos. Environ.,* 38,

569   953-961.

570   Wong, J. P., Zhou, S. & Abbatt, J. P. (2015) Changes in secondary organic aerosol composition

571   and mass due to photolysis: relative humidity dependence. *J. Phys. Chem. A.,* 119, 4309-16.

572   Wu, Y., Huang, X., Jiang, Z., Liu, S. & Cui, L. (2020) Composition and sources of aerosol organic

573   matter in a highly anthropogenic influenced semi-enclosed bay: Insights from excitation-

574   emission matrix spectroscopy and isotopic evidence. *Atmos Res.,* 241.

575   Xiao, H. W., Xu, Y. & Xiao, H. Y. (2023) Source apportionment of black carbon aerosols in winter

576   across China. *Atmos. Environ.,* 298.

577   Xiao, R., Takegawa, N., Zheng, M., Kondo, Y., Miyazaki, Y., Miyakawa, T., Hu, M., Shao, M.,

578   Zeng, L., Gong, Y., Lu, K., Deng, Z., Zhao, Y. & Zhang, Y. H. (2011) Characterization and

579   source apportionment of submicron aerosol with aerosol mass spectrometer during the

580   PRIDE-PRD 2006 campaign. *Atmos. Chem. Phys.,* 11, 6911-6929.

581   Yao, P., Huang, R. J., Ni, H. Y., Kairys, N., Yang, L., Meijer, H. A. J. & Dusek, U. (2022) 13C

582   signatures of aerosol organic and elemental carbon from major combustion sources in China

583   compared to worldwide estimates. *Sci. Total Environ.,* 810.

584   Zaryab, A., Nassery, H. R., Knoeller, K., Alijani, F. & Minet, E. (2022) Determining nitrate

585   pollution sources in the Kabul Plain aquifer (Afghanistan) using stable isotopes and Bayesian

586   stable isotope mixing model. *Sci. Total Environ.,* 823.

587   Zhang, Y. L., Li, J., Zhang, G., Zotter, P., Huang, R. J., Tang, J. H., Wacker, L., Prevot, A. S. &

588   Szidat, S. (2014) Radiocarbon-based source apportionment of carbonaceous aerosols at a

589   regional background site on Hainan Island, South China. *Environ. Sci. Technol.,* 48, 2651-9.

590   Zhao, Y. L., Hennigan, C. J., May, A. A., Tkacik, D. S., de Gouw, J. A., Gilman, J. B., Kuster, W.

591   C., Borbon, A. & Robinson, A. L. (2014) Intermediate-volatility organic compounds: a large

592   source of secondary organic aerosol. *Environ. Sci. Technol.,* 48, 13743-13750.

593   Zhu, Q., He, L. Y., Huang, X. F., Cao, L. M., Gong, Z. H., Wang, C., Zhuang, X. & Hu, M. (2016)

594   Atmospheric aerosol compositions and sources at two national background sites in northern

595   and southern China. *Atmos. Chem. Phys.,* 16, 10283-10297.